Stability Improvement of Isolated Multiple-Output DC/DC Converters Using Coupled Inductors

Esteban Sanchis-Kilders, *Senior Member, IEEE,* Agustín Ferreres, José L. Gasent-Blesa, *Member, IEEE,* Enrique Maset, *Member, IEEE,* Vicente Esteve, *Senior Member, IEEE,* José Jordán, *Senior Member, IEEE,* Juan B. Ejea

***Abstract*—Coupling output inductors is a very popular solution when designing a multiple output DC/DC system. Space-borne circuits are one of the areas where a custom DC/DC converter design with coupled inductors could be preferred, because it allows a detailed design of all variables. Output voltage regulation can be improved using coupled output inductors on a multiple output DC/DC converter and as demonstrated in this paper it provides an enhanced stability. This paper presents the small signal analysis of a push-pull converter with seven outputs having all its output inductors coupled together and compares it theoretically to the uncoupled version to demonstrate the stability improvement. The theoretical results are validated by simulating a linear model of the circuit and measuring the frequency response on an experimental prototype. Design guidelines and additional benefits of output coupled inductors are also discussed.**

***Index Terms*—space power converters, multiple outputs, coupled inductors, small signal analysis, stability**

I. Introduction

THE use of coupled inductors applied to interleaved topologies has been studied in [1] [2] [3]. Some topologies are even based on their behavior, like the Cuk converter [4]. When used in interleaved topologies, coupled inductors reduce response time under a load step [1]. Coupled inductors have also been applied to multiple output converters usually applying weighted control [5] [6] [7] [8] and an improvement of cross regulation has been demonstrated [5]. Without weighted control, other solutions could be applied (robust control) [9] [10] to improve cross regulation, although increasing the complexity of the control circuit. An additional advantage of using coupled inductors is the saving of volume, which for some applications, like space-borne systems, is definitely an important argument.

In [7] a small signal analysis of a coupled inductor forward converter is presented and the transfer functions for a two outputs case are studied. It is stated that the behavior of both outputs is different and depends on the existence of an interlaced pole-zero pair. The two coupled inductors case, where a single coupling coefficient is present simplifies the equations, but in a more complex case with more than two coupled inductors, the coupling coefficient, k, becomes a matrix [5] that represents the coupling of each winding to any other. In this case the previous study is not useful, because the transfer function becomes a matrix equation, and no graphical representation of the transfer function with respect to the coupling coefficient k is possible, as k is not a scalar anymore. In [8], the same authors provide a study including peak current mode control, but not giving more information than already found in [7]. Both papers propose a design guideline for the controller to stabilize the control loop, based on the interlaced pole-zero pair for weighted control.

In [3] a small signal analysis of a multiphase BOOST converter with coupled inductors can be found and here a comparative study of uncoupled and coupled inductors is presented. It is not clear if the authors consider a coupling coefficient matrix or a scalar coupling coefficient. Unfortunately the results of this detailed study can not be directly used for a multiple output BUCK type converter.

Other uses of coupled inductors like in photovoltaic systems and its advantages are described in [11], where zero ripple in the source current is achieved by design.

Due to the lack of a generalized small signal study with more than two coupled inductors for a multiple output BUCK type converter and a comparison of the influence of coupling inductors in the stability itself, the authors present in this paper a theoretical study together with an experimental validation to demonstrate the stability improvement gained with more than two coupled inductors.

This paper presents a detailed study of the small signal analysis of seven coupled inductors used together with primary peak current control in BUCK type, galvanic isolated, multiple output converters. The model has been simulated and experimentally validated with a converter that is the Power Converter Module (PCM) of a real space application. A detailed description and more practical information of the PCM of the Polarimetric and Helioseismic Imager (PHI), instrument to fly on board of the Solar Orbiter satellite (SO) was already published in [12]. The paper demonstrates possible instabilities due to multiple resonances that disappear when coupling inductors together. Other benefits, like independence of the output filter resonances are also achieved and the value of the equivalent primary inductances is also calculated to ease the design of the current loop.

Esteban Sanchis-Kilders, Agustín Ferreres, Enrique Maset, Vicente Esteve, José Jordán and Juan B. Ejea are with the Dpt. de Ingeniería Electrónica, Universidad de Valencia,Valencia, SPAIN. e-mail: esteban.sanchis@uv.es.

José L. Gasent-Blesa is with the Image Processing Laboratory, Universidad de Valencia, Valencia, SPAIN.

This research has been supported by the M. de Economía y Competitividad of Gobierno de España and FEDER, under project ref. AYA2011-29833-C06-06, AYA2012-39636-C06-03 and ESP2013-47349-C6-5-R and partially by the Generalitat Valenciana (D.G.U.ES.C.), under project ref. PROMETEO/2012/044.

Manuscript received January, 2015; revised November, 2015.

II. Power converter Module

The driver of this study has been the design of the PCM. The PCM is based on a push-pull topology with seven outputs using a single transformer and a single output coupled inductor (see Fig. 1), mainly to save volume, but as this paper will demonstrate, coupled inductors also improve stability. The PCM is a custom design system providing seven output voltages (+ 3.4 V, + 6.4 V, − 6.4 V, + 14 V, − 14 V, + 60 V and primary auxiliary + 14 V) with galvanic isolation. In addition, two + 28 V output voltages are delivered from the PCM primary side (28 V bus voltage) for the Mechanisms and Heaters of the instrument (not shown in Fig. 1). These two outputs are not considered in the study, as they do not pass through the DC/DC converter. The PCM manages a maximum power of around 35 W.

The PCM not only includes the DC/DC converter, but also protections, inrush current control, dedicated input filter and a whole power distribution unit on its output to properly supply all required voltages to each user.

The engineering model (EM) of the PCM was already built and is shown in Fig. 2.

The EM of the PCM (Fig. 2) was used to measure the experimental results presented at the end of the paper. Therefore not just a simple breadboard was used to validate the theoretical results but a real space-borne subsystem (with more than 1200 components on a double sided PCB). This has allowed to verify the effect of all additional circuitry on the small signal analysis and how to model this effect in a simulation.

A. Coupled Inductors

Some guidelines are provided for the design of a seven winding coupled inductor. Many of them are similar to a transformer design. These guidelines are based on trade offs made after experimental prototyping.

- Turns' ratio of the coupled inductor should be the same as the turns' ratio of the transformer for each output [5] [13]. This assures that the theoretical volt-second balance applied to each winding is the same (neglecting second order effects like duty cycle loss due to leakage inductance, etc.).
- Coupling windings tight together improves cross regulation, but when involuntary volts-second unbalance is applied to the winding, high di/dt in the current through each output can appear. This could lead to noise problems. Another reason to relax coupling factor is the need, anyway, of post regulators to comply with the required tight regulation.
- Keep turns' number as small as possible. This also reduces the layers and reduces parasitic capacitance.
- Choose core types with as high permeability as possible to decrease the number of turns for the same magnetic inductance. But remember that the core has to sustain the DC current of all outputs.
- Spread windings as much as possible over the whole core, trying to avoid layers, if possible, to reduce parasitic capacitance.
- Finish windings of higher voltage at different ends of the core to reduce parasitic capacitance. But this can increase leakage inductance.

Some more information can be found in [12].

III. Small Signal Analysis

For the theoretical study, the transformer has been supposed ideal (although the linearized simulation model includes duty cycle losses on the transformer's output, due to its leakage inductance, based on experimental measurements) and the coupled inductor real. The model used for the coupled inductor is the inductance matrix, which mathematically suits best for the whole equations deduction and is the real and exact description of a coupled inductor (neglecting parasitic elements like capacitances). Measuring the inductance matrix has to be done very carefully [6] [14] and the proof that demonstrates that the matrix is physically feasible is that its eigenvalues are all real and positive as demonstrated in [15].

A. Procedure

The next steps have been followed to study the small signal behavior of the PCM.

1) The small signal analysis of a simplified BUCK-type converter with coupled inductors has been done.
2) The linearized model has been studied including the experimentally measured coupling inductance matrix.
3) The resulting equations have been particularized for no coupling (changing all mutual inductances of the inductance matrix to zero; the inductance matrix becomes then diagonal) and compared graphically to the previous obtained transfer functions.
4) A linearized model has been simulated with SPICE to validate the theoretical model.
5) The SPICE model has been made more real adding parasitic elements and other real components, like input filter, duty cycle loss due to the transformer's leakage, parasitic resistance of tracks of the PCB, of the current sensing shunts used in the PCM and others.
6) The frequency response of the complex SPICE model and the experimentally measured frequency response has been compared (of course, the more complex model is based on the simplified theoretical model).

B. Analysis

The small signal analysis is based on well known averaging techniques. Taking into account that the Push-Pull converter is a BUCK type topology and that in our case all output inductors are coupled together, only the secondary side of the j-th output is shown in Fig. 3 and used for the analysis.

In Fig. 3, switching action has already been linearized and the input transformer has also been converted into a DC transformer, that includes not only the turns ratio but also the effect of the duty cycle. We use matrix algebra to analyze the circuit to take into account the fact that all outputs are coupled together and therefore influence each other. The sub-indexes of the matrices are j and k and both vary from 1 to 7. Of

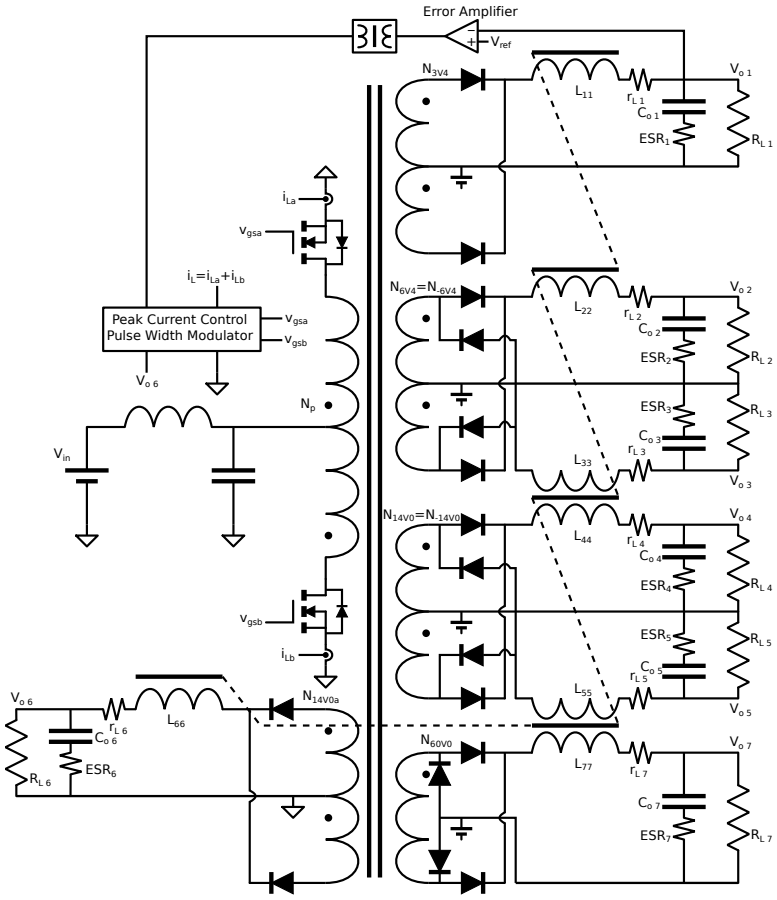

Fig. 1. Simplified schematic of the power section (Push-Pull topology) of the PCM converter. The turns' ratio of the negative voltages is the same as for the positive voltages. In fact, negative and positive outputs share the same winding. The error amplifier has also been simplified and the feedback impedances are not shown.

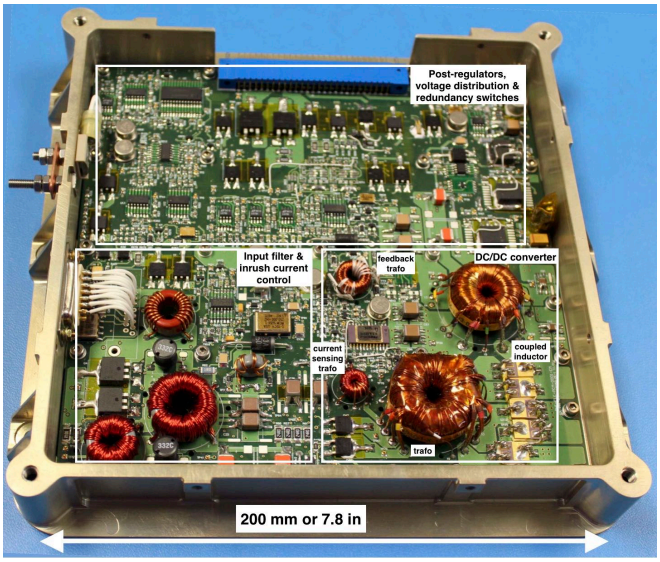

Fig. 2. Engineering Model of the PCM. On the right side of the picture, the coupled inductor can be seen and below it the main transformer. The three ring cores on the left belong to the input filter and the two small ring cores in the middle are the magnetic feedback and the current sensing transformer.

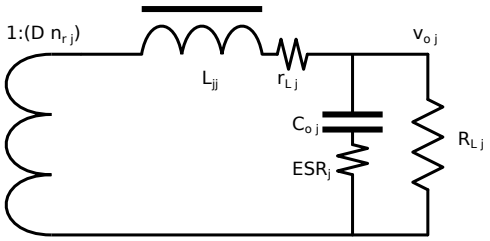

Fig. 3. Small signal model of the j-th output of the push-pull converter. D is the duty cycle, $n_{r\,j}$ is the turns' ratio, $v_{o\,j}$ is the output voltage, L_{jj} is the self inductance, $C_{o\,j}$ is the output capacitor, $R_{L\,j}$ is the load resistance, $r_{L\,j}$ is the parasitic series resistance of the inductance and ESR_j is the equivalent series resistance of the output capacitor.

course, the dimensions of the matrices that appear in these formulae are equal to the number of coupled inductors of the converter and are equal to seven in our case.

Once the inductance matrix, $\mathbf{L_o}$, is known (both, mutual inductances, L_{jk}, and self-inductances, L_{jj}) it has to be checked if the matrix is physically feasible. The mathematical condition is that the eigenvalues are real and positive [6].

For our calculation we must also know the turns' ratio of each secondary to primary, written in vector form, $\mathbf{n_r}$.

$$\mathbf{n_r^T} = \frac{1}{N_p}\left(N_{3V4}\ N_{6V4}\ N_{-6V4}\ N_{14V0}\ N_{-14V0}\ N_{14V0a}\ N_{60V0}\right) \quad (1)$$

N_p is the primary turns' number and N_{xVy} is the turns'

number of each of the secondaries. The coupling coefficient matrix, which is necessary to couple inductances together in SPICE, is defined as,

$$k_{jk} = \frac{L_{jk}}{\sqrt{L_{jj} L_{kk}}} \tag{2}$$

It describes the coupling of each winding to each other [14]. But two things have to be kept in mind:

- k_{jk} must never be larger than one;
- SPICE simulators will not simulate a coupled inductor whose coupling coefficient matrix corresponds to an inductance matrix that has wrong eigenvalues (not all positive and real).

If the feasibility probe has been passed, then the coupling coefficients will be correct.

Matrix calculus is applied and the impedance matrix of all outputs, taking into account that all inductors are coupled together, is:

$$Z_{LRC\,jk}(s) = \begin{cases} L_{jj}s + r_{L\,j} + Z_{RC\,j}(s) & \text{if} \quad j = k \\ L_{jk}s & \text{if} \quad j \neq k \end{cases} \tag{3}$$

where,

$$Z_{RC\,j}(s) = \left(\frac{1}{C_{o\,j}s} + ESR_j \right) \parallel R_{L\,j}(s) \tag{4}$$

and r_{Lj} is the parasitic series resistance of the inductance, L_{jj} is the self inductance and $Z_{RC\,j}$ is the output impedance of each output taking into account the output capacitance $C_{o\,j}$, its equivalent series resistance ESR_j, and the load resistance, R_L, all associated to the j-th winding (Fig. 3).

The next step is to calculate the admittance of each output taking into account that the inductors are coupled and that the turns' ratio of each coupled inductor is the same as the corresponding turns' ratio of the transformer, $n_{r\,j}$, and reflects each of the admittances to primary using the square of the turns' ratio, $n_{r\,j}^2$.

The resulting primary admittance vector, $\mathbf{Y_{LRC\,p}}(s)$, is,

$$Y_{LRC\,p\,j}(s) = n_{r\,j} \sum_k n_{r\,k} \, [\mathbf{Z_{LRC}}(s)^{-1}]_{jk} \tag{5}$$

Adding them together results in the equivalent input admittance on primary side, $Y_i(s)$, (the input impedance corresponds to its inverse value).

$$Y_i(s) = \sum_j Y_{LRC\,p\,j}(s) \tag{6}$$

The Bode plot of these admittances, $Y_{LRC\,p\,j}(s)$, is shown in Fig. 4, together with the total input admittance, $Y_i(s)$, for coupled and uncoupled inductors. To represent the uncoupled case in Fig. 4, the whole equation set has been taken, but changing the inductance matrix, $\mathbf{L_o}$, by making all its mutual inductances equal to zero.

It is interesting to see that each of the elements of $\mathbf{Y_{LRC\,p}}(s)$ shows a second group of resonances (poles and zeros) due to the coupling effect (already described in [7] [8]), but the main resonant frequency is the same for all

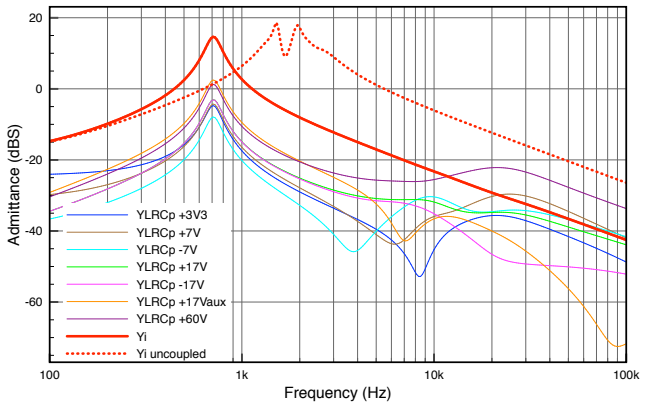

Fig. 4. Primary input admittance, $Y_{LRC\,p\,j}$, of all outputs and the total input admittance, Y_i. The uncoupled total input admittance is also shown. The coupled input admittance naturally cancels out the second resonances seen around 8 kHz and has a unique main resonance. The uncoupled input admittance has no second resonances but has no unique main resonance.

and corresponds to the equivalent primary output capacitance (reflecting all capacitors to primary) and an equivalent primary inductance defined later on (see Eq. (7)). It is also interesting that the sum of all these admittances, with its corresponding turns' ratio factor, $Y_i(s)$, cancels out naturally this additional second group of resonances (poles and zeros). This, on the other hand agrees with the single scalar inductance seen on the primary side (Eq. (7)). It is also important to highlight that the equivalent inductance is not the parallel connection of all self-inductances, but depends on the mutual inductances and therefore their coupling coefficient. It can be much larger than the parallel connection of all self-inductances. This can dramatically lower the slope of the primary current and this has to be taken into account when designing the peak current control.

As already demonstrated in [8], weighted control can balance the external voltage loop and further compensate the effect of this resonances' group. But in our case only one output voltage is fed back and therefore a careful analysis has to be fulfilled to assure stability. These resonances become the more critical the lower their frequencies are as they can interfere with the crossover frequency and they also move with k as running variable (see [8] for more details), if a two winding coupled inductor is supposed. But as coupling coefficient is not unique (it is a matrix), this design procedure cannot be used with many windings. In fact, it is difficult to design for a given coupling coefficient and almost impossible to design for a given coupling coefficient matrix.

It is possible to calculate the equivalent inductor seen on the primary side ($L_{o_{primary}} \equiv L_p$) based on the coupled inductors matrix and the turns' ratio, taking into account that the turns' ratio of the transformer is the same as the turns' ratio of the coupled inductors. The value of $L_{o_{primary}}$ (also referred to as L_p in the following equations for simplicity purposes) is given in Eq. (7) and it is needed to design the current loop and calculate the primary current slope,

$$L_{o_{primary}} \equiv L_p = \frac{1}{\mathbf{n_r^T L_o^{-1} n_r}} \tag{7}$$

The duty-to-inductor-current transfer function can be calculated for the total primary current, $G_{d\,i_{L_p}}(s)$, and for the secondary current of a single output, $G_{d\,i_{L_j}}(s)$ taking into account the equivalent admittance, $Y_{LRC\,p\,j}(s)$ and Fig. 3.

The transfer function of inductor current of the j-th output related to the duty cycle is (V_{in} is the input voltage),

$$G_{d\,i_{L_j}}(s) = \frac{\hat{i}_{L\,j}}{\hat{d}} = \frac{V_{in} Y_{LRC\,p\,j}(s)}{n_{r\,j}} \tag{8}$$

And the overall primary current transfer function $G_{d\,i_{L_p}}(s)$, is.

$$G_{d\,i_{L_p}}(s) = \frac{\hat{i}_{L_p}}{\hat{d}} = \sum_j n_{r\,j}\; G_{d\,i_{L_j}}(s) = V_{in} Y_i(s) \tag{9}$$

This transfer function corresponds to the power section and it has to be highlighted that coupling output inductors naturally cancels second resonances out and provides only one unique main resonance (see Fig. 4).

IV. Loop Transfer functions

The regulation is based on a peak current loop that measures the primary current that is controlled by an outer voltage loop that senses the + 3.4 V output (highest power output, 20 W). The + 3.4 V output feeds a digital load that requires a very tight regulation.

Well known control theory [7] [8] [9], has been applied and some parasitic elements (resistances) have been taken into account. Influence of the parasitic capacitance of the magnetic elements has been neglected and the main transformer has been supposed to be ideal.

One critical point is that the current loop senses the primary side current, i.e. overall current of the secondary side reflected to primary. The primary current waveform and as expected from Eq. (7), has a triangular shape resulting from the addition of all secondary currents that cancels the non-pure-triangular waveform shape that usually appears on coupled inductors (due to volt-second unbalances). Another point is that in our design the voltage loop is closed around the low voltage-high current-highest power output, v_{o1} (3.4 V). No weighted control was used, as tight regulation was necessary on the v_{o1} output and linear post regulators were used on the other outputs where good regulation was needed. Anyhow, the reduction of cross-regulation with the help of coupled inductors reduces the losses of these post regulators.

A. Block diagram

The control block diagram used to deduce the different transfer functions is shown in Fig. 5.

The different blocks shortcuts used in Fig. 5 correspond to classical peak current control: $\mathbf{FM}$ is the modulator transfer function, $\mathbf{He}$ is the sampling effect and $\mathbf{Rs}$ is the sensing resistor (definition following [8]). The different transfer functions are named with the capital letter $\mathbf{G}$ and the sub-index indicates the input and output variable (see Eq. (8) and Eq. (9)). To clearly identify primary and secondary currents

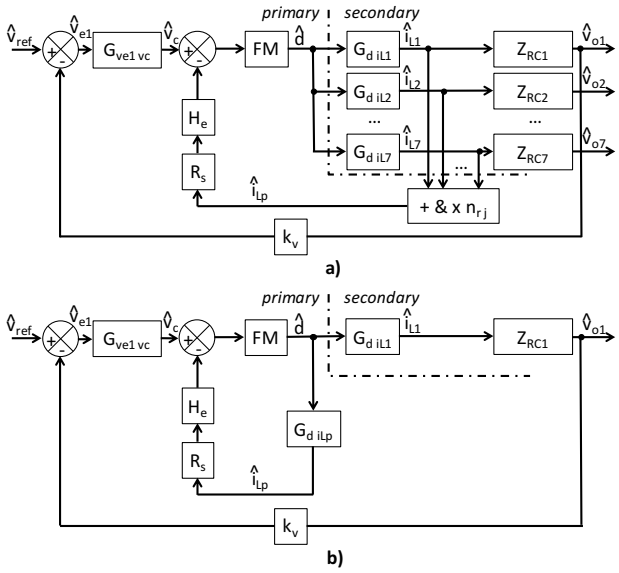

Fig. 5. Control block diagram. a) General diagram, where ($+$ & $\times\, n_{r\,j}$) means that the secondaries are added together ($+$), each with its corresponding transfer ratio ($\times n_{r\,j}$). b) Simplified diagram that uses the primary current transfer function as defined by Eq. (9).

the current adding block in Fig. 5 a) includes the turns ratio $n_{r\,j}$. Therefore, $\hat{i}_{L_j}$ are secondary currents and $\hat{i}_{L_p}$ is the primary current. The modulator transfer function, $\mathbf{FM}$, defined by Eq. (10), includes the switching frequency, f_s, the sensed ON current slope and the maximum compensation ramp (that corresponds to the OFF current slope). $\mathbf{FM}$ is referred to primary current and the difference between coupled and uncoupled version would only be the value of L_p.

$$FM = \frac{f_s}{R_s \frac{V_{in}}{L_p}} \tag{10}$$

B. Transfer function

The next step is to obtain the equivalent transfer function for the current loop following the block diagram shown in Fig. 5.

$$T_i(s) = R_s\, H_e(s)\, FM\, G_{d\,i_{L_p}}(s) \tag{11}$$

Now, the open loop gain of the voltage loop has to be obtained. Taking into account that the closed current loop is controlled only by one output error voltage that depends on its output voltage, and this voltage on its own output current flowing into the output impedance, we can simplify the block diagram of Fig. 5 a) to b) and deduce,

$$\begin{aligned} G_{v_c\,i_{L1}}(s) = \frac{\hat{i}_{L1}}{\hat{v}_c} &= \frac{FM}{1+T_i(s)} G_{d\,i_{L1}}(s) \\ &= \frac{FM}{1+T_i(s)} \frac{V_{in} Y_{LRC\,p\,1}(s)}{n_{r\,1}} \end{aligned} \tag{12}$$

The final open loop gain of the voltage loop (the function to be compensated to assure stability) is,

$$G_{v_c\, v_{o1}}(s) = \frac{\hat{v}_{o1}}{\hat{v}_c} = G_{v_c\, i_{L1}}(s)\, Z_{RC\,1}(s) \tag{13}$$

The overall open loop gain, T_v, corresponds to Eq. (13) times the PI compensation, $G_{v_{e1}\, v_c}(s)$, and the gain factor, k_v,

$$T_v(s) = k_v\, G_{v_{e1}\, v_c}(s)\, G_{v_c\, v_{o1}}(s) \tag{14}$$

V. Results

In this section, both, theoretical and experimental results will be presented to validate the analysis performed and to show the stability improvement of coupled inductors compared to uncoupled inductors.

A. Simulation results

To verify the theoretical results, some frequency domain simulations have been performed using LTspice™. The switching behavior has been linearized using state-space averaging. Both, the theoretical equations and the simulation model have been used for coupled inductors and uncoupled inductors. To theoretically uncouple the inductors, the inductance matrix has been changed and all its values, but the main diagonal, have been made equal to zero. This will represent the same converter but uncoupling its output inductors. Fig. 6 shows Bode plots of the overall loop gain, T_v, of both cases.

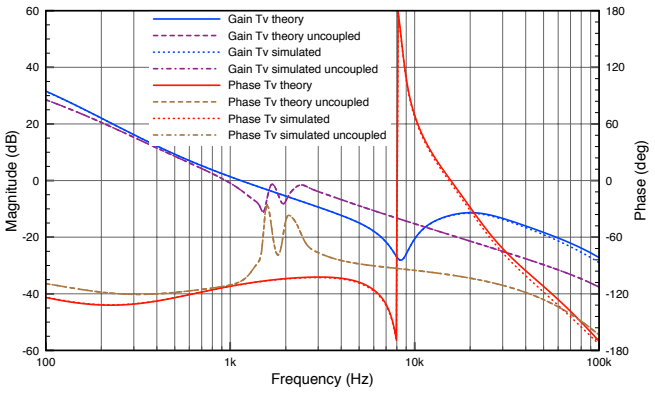

Fig. 6. Comparison of open loop gain (T_v) Bode plots for both, theoretical calculations and ideal simulations. The coupled and uncoupled case is shown. Theory and simulation are identical. The uncoupled model has undesirable resonances close to the crossover frequency, which can jeopardize stability. The coupled model naturally cancels this resonances out and only presents a single resonance at much higher frequencies.

The overall open loop transfer function, T_v, represented by Eq. (14) and shown in Fig. 6, has the proper PI compensation, $G_{v_{e1}\, v_c}(s)$, to achieve 1 kHz bandwidth. It can be seen that simulated and theoretical curves are the same. Both, theoretical and simulated Bode plots take into account the effect of only the following parasitic elements: inductor's series resistance and ESR of the output capacitor.

Comparing both, coupled and uncoupled solution, we see that the uncoupled solution presents some severe resonances at low frequency and close to the cross-over frequency, which will change with the tolerance of the components and value of the parasitic elements. This is not acceptable as it can jeopardize stability. In the case of using coupled inductors, the curves shift this behavior to a single and much higher frequency and therefore does not affect stability. This behavior would clearly favor the use of a coupled inductor solution from the stability point of view. These resonances are directly related to the resonance frequency of each output, which are usually not the same, because the output filter components selection depends on the requirements of the load of the given output. This results in similar but different resonances that add together on the primary, which clearly affects the uncoupled case (see Fig. 4). The coupled inductors solution cancels out naturally these differences of the resonance frequency of the output filters and one single resonance remains, defined approximately by the primary inductance, L_p, (defined by Eq. (7)) and the equivalent primary output capacitance (defined as $C_{o\,p} = \sum_j n_{r\,j}^2 C_{o\,j}$). No parametric Bode plot can be obtained related to coupling coefficient k, as no single k is available, but a whole coupling matrix.

B. Experimental results

The described study was made for the PCM prototype. Therefore experimental results based on the prototype of the PCM (see Fig. 1) were measured.

The main characteristics of the prototype are given in the following tables.

TABLE I
Experimental power stage data

V_{in}	$V_{in\ nominal}$	f_s	N_p
$26\ V \ldots 29\ V$	$28\ V$	$250\ kHz$	10

TABLE II
Experimental output voltages data

secondaries	$V_{o\,j}$	L_{jj}	$r_{L\,j}$	$C_{o\,j}$	ESR_j	$R_{L\,j}$	$P_{o\,j}$
$N_{3V4} = 2$	$3.4\ V$	$9.24\ \mu H$	$3\ m\Omega$	$466\ \mu F$	$30\ m\Omega$	$0.66\ \Omega$	$17.5\ W$
$N_{6V4} = 4$	$6.4\ V$	$36.26\ \mu H$	$17\ m\Omega$	$151\ \mu F$	$50\ m\Omega$	$5.7\ \Omega$	$7.2\ W$
$N_{-6V4} = 4$	$-6.4\ V$	$36.26\ \mu H$	$51\ m\Omega$	$104\ \mu F$	$100\ m\Omega$	$16\ \Omega$	$2.6\ W$
$N_{14V0} = 9$	$14.0\ V$	$192.90\ \mu H$	$182\ m\Omega$	$35\ \mu F$	$50\ m\Omega$	$155\ \Omega$	$1.3\ W$
$N_{-14V0} = 9$	$-14.0\ V$	$192.90\ \mu H$	$190\ m\Omega$	$35\ \mu F$	$50\ m\Omega$	$155\ \Omega$	$1.3\ W$
$N_{14V0a} = 9$	$14.0\ V$	$192.90\ \mu H$	$392\ m\Omega$	$67\ \mu F$	$25\ m\Omega$	$310\ \Omega$	$0.6\ W$
$N_{60V0} = 34$	$60.0\ V$	$2741.4\ \mu H$	$1260\ m\Omega$	$4\ \mu F$	$250\ m\Omega$	$2\ k\Omega$	$1.8\ W$

First, the inductance matrix of the seven coupled inductors of the PCM, built using the MPP core 55348 of Magnetics™, was measured. The results of the measured inductance matrix, $\mathbf{L_o}$, and its turn's ratio, $\mathbf{n_r}$, which is the same as the turns' ratio of the transformer, (it can be directly calculated from the values found in table I and table II) are,

$$\mathbf{L_o} = \begin{pmatrix} 9.24 & 18.01 & 17.54 & 41.75 & 41.45 & 41.38 & 157.06 \\ 18.01 & 36.26 & 35.52 & 81.99 & 82.64 & 80.92 & 313.20 \\ 17.54 & 35.52 & 36.26 & 79.01 & 80.35 & 79.67 & 307.92 \\ 41.75 & 81.99 & 79.01 & 192.90 & 188.08 & 187.30 & 717.22 \\ 41.45 & 82.64 & 80.35 & 188.08 & 192.90 & 182.89 & 719.22 \\ 41.38 & 80.92 & 79.67 & 187.30 & 182.89 & 192.90 & 706.99 \\ 157.06 & 313.20 & 307.92 & 717.22 & 719.22 & 706.99 & 2741.4 \end{pmatrix} \mu H \tag{15}$$

$$\mathbf{n_r^T} = (0.2 \quad 0.4 \quad 0.4 \quad 0.9 \quad 0.9 \quad 0.9 \quad 3.4) \tag{16}$$

The equivalent primary inductance, Eq. (7), results then

$$L_{o_{primary}} = 212.2\ \mu H \tag{17}$$

Which, if the output inductor is uncoupled but with the same values (as explained earlier, the inductance matrix is modified, changing all its values to zero except for the main diagonal), the primary inductance is then reduced to,

$$L_{o_{primary\ \ uncoupled}} = 33.4\ \mu H \tag{18}$$

One consequence of having a much larger primary inductance when using coupled inductors is that the primary side current slope is much lower and that the magnetizing inductance of the transformer can be of the same order of magnitude. This also leads to the design option of reducing the output inductor needed to keep the same current ripple or to keep the inductor of the same value but being able to achieve lower output currents without leaving continuous conduction mode. In fact, this last option was our design choice.

Finally, the frequency response of the converter with the control already described, was measured and compared to the model.

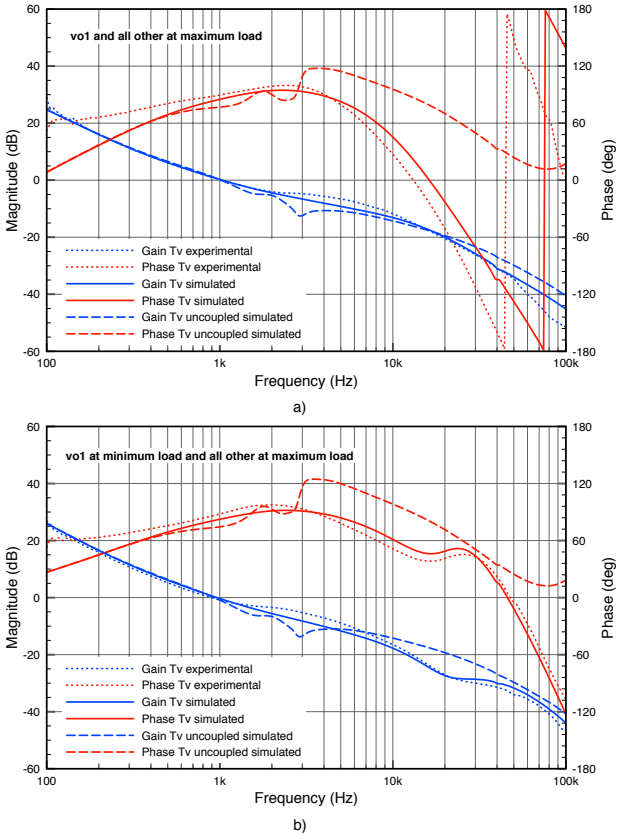

Fig. 7. Simulated (with coupled and uncoupled inductors) and measured (only for coupled inductors) open loop (T_v) frequency response of the real converter for two different load conditions. Gain and phase (+180°) of T_v are shown. a) corresponds for maximum load at all outputs and b) has minimum load at the v_{o1} output and all other outputs at maximum load.

Fig. 7 shows the comparison of the measured and simulated frequency response of the open loop gain. For this simulation, the previous derived SPICE model has been used but with some substantial modifications to achieve a more real behavior. The following elements have been added: the parasitic elements of the tracks of the PCB, the rectifying diodes with their small signal model, the duty loss due to the leakage inductance of the transformer, the input filter of the converter and the real opamp model for the PID compensator. The coupled inductor value was slightly reduced, taken into account that DC current flowing through it would reduce the value of A_L of the ring core used. For the uncoupled simulation, the coupling factor, k_{ij}, has been made equal to zero for all inductors. The agreement of both curves, simulated and experimental for coupled inductors, is very good taking into account that the measurement was done on a real converter with its full complex output loads (post regulators, different output sensors, output switches, etc. [12]). To validate the model, two different load conditions were simulated and tested, and the agreement remains very good. The simulated frequency response of the overall gain, T_v, for uncoupled inductors, although very damped, still exhibits the resonance frequencies, which in this case does not affect the stability, but is clearly an undesirable effect because it is very difficult to predict and the parasitic elements that influence and damp it can neither be designed nor controlled.

Due to the complexity of the prototype (see Fig. 2) it has not been possible to experimentally measure the frequency response of the overall open loop gain, T_v, when using uncoupled inductors.

C. Design guidelines

The results presented leads us to recommend the use of coupled output inductors in multiple output converters, because

- this simplifies the resonance of the all the output filters
- the equivalent primary inductor is a larger single value
- the frequency response improves and only a single resonance appears, related to the equivalent primary inductance
- a simple coupled inductor design can be followed

Therefore, the design should follow the classical converter design. Then the inductance of the highest output power should be designed and later all other inductors are just added by winding just the number of turns dictated by the turns ratio of the transformer for each output. Of course the core must be selected to cope with the energy of all outputs together and must provide a large enough window to house all the windings. The most critical parameter is the parasitic capacitance of the the coupled inductor, which has to be kept small.

VI. Conclusions

A real, seven-output BUCK type power converter designed for space applications, using coupled inductors has been presented and its control loop analyzed in detail.

A short discussion on the use of coupled inductors has been presented. A generalized small signal analysis has been performed based on real coupling of all the inductors, where all inductors exhibit a different coupling coefficient to each other.

The equivalent primary inductance of the coupled inductor has been calculated. It has been demonstrated that it is a

scalar derived from a matrix equation. Real values predict that coupling inductors together increases the primary inductance compared to using uncoupled inductors of the same value. This allows either to stay in continuous conduction mode with less DC current or reducing the inductance and therefore its size.

The small signal analysis has shown that a coupled inductor provides a frequency response that, when reflected to primary, naturally cancels out all secondary cross resonances and results in a clean second order response, fact that does not happen with the uncoupled version. This results in a cleaner overall frequency response that is more stable for a double loop control (inner overall current loop and outer voltage loop) than an uncoupled solution (if the inductance values are kept the same). The stability is also enhanced when coupling output inductors together because output filter resonances are unified and its dependence on component value' tolerances can therefore be neglected. The paper describes the mathematical model that allows verifying stability for both cases.

Real prototypes can hide multiple resonances if large parasitic resistances damp them. The theoretical small signal model of the PCM has been modified by adding all parasitic elements to reproduce the behavior of the real circuit. The experimental data matches the simulated prediction. The uncoupled circuit has also been simulated to show its effect and conclude that, although stable, it can be conditionally stable as it relies on parasitic elements for damping the resonances. Relying on parasitic elements to damp potential harmful resonances is not desirable in space applications where long term stability is needed. Parasitic elements are by definition very difficult to predict.

ACKNOWLEDGMENT

The authors would like to thank, Mr. D. Osorno and Mr. D. Gilabert for their help with the experimental prototype.

REFERENCES

[1] G. Zhu, B. McDonald, and K. Wang, "Modeling and analysis of coupled inductors in power converters," *Power Electronics, IEEE Transactions on*, vol. 26, no. 5, pp. 1355–1363, 2011.

[2] H. B. Shin, J. G. Park, S.-K. Chung, H. W. Lee, and T. Lipo, "Generalised steady-state analysis of multiphase interleaved boost converter with coupled inductors," *Electric Power Applications, IEE Proceedings* -, vol. 152, no. 3, pp. 584–594, 2005.

[3] H. B. Shin, E.-S. Jang, J. G. Park, H. W. Lee, and T. Lipo, "Small-signal analysis of multiphase interleaved boost converter with coupled inductors," *Electric Power Applications, IEE Proceedings* -, vol. 152, no. 5, pp. 1161–1170, 2005.

[4] V. Vorperian, "The effect of the magnetizing inductance on the small-signal dynamics of the isolated cuk converter," *Aerospace and Electronic Systems, IEEE Transactions on*, vol. 32, no. 3, pp. 967–983, July 1996.

[5] D. Maksimovic, R. Erickson, and C. Griesbach, "Modeling of cross-regulation in converters containing coupled inductors," *Power Electronics, IEEE Transactions on*, vol. 15, no. 4, pp. 607–615, 2000.

[6] R. Erickson and D. Maksimovic, "A multiple-winding magnetics model having directly measurable parameters," in *Power Electronics Specialists Conference, 1998. PESC 98 Record. 29th Annual IEEE*, vol. 2, May 1998, pp. 1472–1478.

[7] Q. Chen, F. Lee, and M. Jovanovic, "Small-signal analysis and design of weighted voltage control for a multiple-output forward converter," *Power Electronics, IEEE Transactions on*, vol. 10, no. 5, pp. 589–596, 1995.

[8] ——, "Current-mode control for multiple-output converters," *Aerospace and Electronic Systems, IEEE Transactions on*, vol. 32, no. 4, pp. 1412–1420, 1996.

[9] D. Cerver, G. Garcera, E. Figueres, J. M. Benavent, and M. Pascual, "Analysis and design of a robust model-following control circuit for multiple-output isolated dc-dc converters with current injection control," in *Power Electronics Specialists Conference, 2004. PESC 04. 2004 IEEE 35th Annual*, vol. 1, June 2004, pp. 171–177 Vol.1.

[10] G. Garcera, E. Figueres, M. Pascual, and J. Benavent, "Robust model following control of parallel buck converters," *Aerospace and Electronic Systems, IEEE Transactions on*, vol. 40, no. 3, pp. 983–997, 2004.

[11] M. Veerachary, "Power tracking for nonlinear pv sources with coupled inductor sepic converter," *Aerospace and Electronic Systems, IEEE Transactions on*, vol. 41, no. 3, pp. 1019–1029, July 2005.

[12] E. Sanchis-Kilders, A. Ferreres, E. Maset, J. Ejea, J. Gasent-Blesa, V. Esteve, J. Jordan, A. Garrigos, and J. Blanes, "On the design of a multiple-output dc/dc converter for the phi experiment on-board of solar orbiter," in *Applied Power Electronics Conference and Exposition (APEC), 2013 Twenty-Eighth Annual IEEE*, March 2013, pp. 3305–3310.

[13] L. H. Dixon, "Coupled inductor design," Texas Instruments, TI Literature Number: SLUP105, 1993 Texas Instruments Power Supply Design Seminar SEM900, Topic 8, 1993.

[14] B. Hesterman, "Analysis and modelling of magnetic coupling," Advanced Energy Industries, www.denverpels.org, Tech. Rep., 2007.

[15] Y. Tokad and M. B. Reed, "Criteria and tests for readability of the inductance matrix," *American Institute of Electrical Engineers, Part I: Communication and Electronics, Transactions of the*, vol. 78, no. 6, pp. 924–926, 1960.

Esteban Sanchis-Kilders (M'00-SM'14) was born in Valencia, Spain, on January 2, 1967. He received the M.Sc. degree in physics, with specialization in electronics, and the Ph.D. degree from the University of Valencia, Spain, in 1990 and 1997, respectively. His employment experience includes one year with GH Industrial S.A., two years with the Power Conditioning Section of the European Space Agency (Noordwijk, The Netherlands), and five years as an Assistant Professor at the University of Valencia. He is currently an Associate Professor at the University of Valencia, where he is also a member of the Laboratory of Industrial Electronics and Instrumentation. His main research interests are space power systems and industrial applications.

Agustín Ferreres was born in Sant Mateu, Spain, on November 26, 1963. He received the M.Sc. degree in physics (with specialization in electronics) and the Ph.D. degree in electronic engineering from the University of Valencia, Spain, in 1993 and 1999, respectively. For two years, he was a Power Electronics Researcher with the R+D Department of GH Industrial S.A. In 1995, he joined the Laboratory of Industrial Electronics and Instrumentation of University of Valencia, where he is currently an Associate Professor. His research interests include space power systems, power supplies and industrial applications.

José L. Gasent-Blesa (M'12) was born in Llíria, Spain. He received the M.Sc. degree in telecommunication engineering from the Polytechnic University of Valencia, Spain, in 1999, and a M.A.Sc. in electronic engineering from the University of Valencia, in 2009. His employment experience include more than 15 years involved in space payload development. He is currently the Project Manager of the PHI instrument (for Solar Orbiter satellite) at the University of Valencia. His main research interests are space systems, reliability and power electronics.

Enrique Maset (M'00) was born in Xàtiva, Spain, in October 1965. He received the M.Sc. and Ph.D. degrees in physics from the University of Valencia, Spain, in 1988 and 1993, respectively. He is currently an Associate Professor in the Department of Electronic Engineering at the University of Valencia, Spain, where he is also a member of the Laboratory of Industrial Electronics and Instrumentation. His main research areas are space power systems and static and dynamic characterization of electronic power devices.

Vicente Esteve (M'03-SM'14) was born in Valencia, Spain, in 1961. He received the M.Sc. and Ph.D. degrees from the University of Valencia, Spain, in 1986 and 1999, respectively. He is member of the Department of Electronic Engineering, University of Valencia, where he is currently an Associate Professor. His research activities include high-frequency rectifiers and inverters for industrial applications, high-power inverters for induction heating, and electronic instrumentation. He is a consultant of several electronics companies in the field of power supplies and advanced topologies. He has more than 20 years of experience on the design and testing of power electronic equipment.

José Jordán (M'08-SM'15) was born in 1964. He received the M.Sc. degree in physics with specialization in electronics and the Ph.D. degree in electronic engineering from the University of Valencia, Spain, in 1989 and 2003, respectively. From 1987 to 2001, he held research positions at GH Electrotermia, where his activities were focused on the design of high-frequency and high-power converters. He is currently an Associate Professor with the University of Valencia. His research interests are power semiconductor characterization and power converters. In these areas, he is frequently a consultant to industrial concerns.

Juan B. Ejea was born in Xàtiva, Spain, on June 27, 1969. He received the M.Sc. degree in physics, with specialization in electronics, and the Ph.D. degree in electronic engineering from the University of Valencia, Spain, in 1993 and 2000, respectively. His employment experience include two years with GH Industrial S.A., two years with the Power Section of the European Laboratory for Particle Physics (CERN), Geneva, Switzerland, and five years as an Assistant Professor at the University of Valencia. He is currently an Associate Professor at the University of Valencia, where he is also a member of the Laboratory of Industrial Electronics and Instrumentation. His main research interests are space power systems and industrial applications.